

## Collisional simulations of the modulator section in coherent electron cooling

A. Al Marzouk<sup>\*</sup> and B. Erdélyi

*Department of Physics, Northern Illinois University, DeKalb, Illinois 60115, USA*

 (Received 15 December 2023; accepted 11 March 2024; published 5 April 2024)

The first section of any coherent electron cooling (CeC) system is the modulator, where the density of the electron beam is modulated by the copropagating ion beam. This density modulation is a result of Coulomb collisions between the individual particles of the two beams. The pairwise, stochastic part of the interactions impacts the overall performance of the CeC process. We present the first simulations of the density modulations of the electron beams from a collisional picture of the dynamics, considering the proof-of-principle CeC experiments at Brookhaven National Laboratory. These simulations were performed using PHAD, which is the first efficient, large-scale collisional numerical method in beam physics that we have previously developed and benchmarked. Realistic beam distributions and external fields have been optimized to provide strong modulation signals necessary for variations of coherent electron cooling systems. Cooling performance limits and potential collisionless simulation pitfalls are pointed out.

DOI: [10.1103/PhysRevAccelBeams.27.044401](https://doi.org/10.1103/PhysRevAccelBeams.27.044401)

### I. INTRODUCTION

Modern colliders, such as the electron-ion collider (EIC) at Brookhaven National Laboratory (BNL) [1], require high-intensity, high-energy hadron beams for advancing nuclear physics. An important figure of merit for such colliders is high luminosity, which can be achieved by a cooling technique that decreases the phase space volume of the beam, or the beam emittance. There are three well-known methods to cool heavy ion beams: electron cooling, stochastic cooling, and laser cooling [2]. According to [2], electron cooling and laser cooling are more efficient to cool high-intensity, low-energy beams, while cooling low-intensity, high-energy beams is better achieved by stochastic cooling. The two traditional methods that are commonly used and can be considered for EIC are the electron cooling [3,4] and the stochastic cooling [5,6].

In the EIC hadron storage ring, the hadron energies are  $\gg 10$  GeV/nucleon, at which the emittance degrades in about 2 h due to intrabeam scattering (IBS) and other diffusion mechanisms [7]. This calls for strong hadron cooling, where the hadron beam at such energies is cooled with short cooling times ( $\lesssim 1$  h). For intense beams in this high-energy regime, the efficiency of both traditional cooling techniques declines with the increase of energy

for electron cooling and with the increase of intensity for stochastic cooling. Traditional electron cooling relies on dc accelerators, which cannot accelerate electron beams to the required high energies due to technical limitations. In recent years, bunched electron cooling has been demonstrated and is being studied as a candidate to provide high-energy electron beams accelerated by radio-frequency linear accelerators (rf linacs) to cool the hadron beam [8–11].

In traditional stochastic cooling, the particle properties are measured by a pickup operating in the microwave regime, then the signal is amplified and applied as a kick to the particles at a later stage. Because of its dependence on the beam properties, it is limited to cool low-intensity hadron beams and cannot meet the high-intensity requirement. Extending the bandwidths to the higher frequencies of the optical wavelengths in the pickup and kicker stages could enable the cooling of high-intensity beams at a very high cooling rate. This led to the proposal and development of the optical stochastic cooling (OSC) and the coherent electron cooling (CeC). The OSC was proposed about 30 years ago [12,13], but only recently the OSC concept was experimentally demonstrated at the Fermi National Accelerator Laboratory's Integrable Optics Test Accelerator [14].

The CeC concept and its implementation were proposed and discussed in [2] and its practical scheme with a detailed theory appeared in [15,16]. The CeC system consists of three sections: a modulator, an amplifier, and a kicker. Different CeC systems were proposed and theoretically explained, and they vary mainly in the amplification method [17]. The amplifier in the first proposed CeC was the high-gain free electron laser (FEL) [15,16]. Other amplification methods were proposed and studied later, such as the microbunching

<sup>\*</sup>afnan.almarzouk1@gmail.com

*Published by the American Physical Society under the terms of the Creative Commons Attribution 4.0 International license. Further distribution of this work must maintain attribution to the author(s) and the published article's title, journal citation, and DOI.*

instability (MBI) [18] and the plasma cascade instability (PCI) [19]. Because of its high cooling rate, the CeC was chosen as the baseline method of strong hadron cooling at EIC [7]. The CeC proof-of-principle (PoP) experiments were proposed in [20] to test the CeC concept before it can be applied to achieve high luminosity in EIC and were commissioned at the Relativistic Heavy Ion Collider (RHIC) at BNL in recent years.

The first section of any CeC system, the modulator, is based on the Coulomb interactions between the ions and the electrons. The ion beam and the electron beam copropagate in the straight line of the modulator with the same velocity. Each ion attracts the surrounding electrons until the total charge equals that of the ion, but of the opposite sign, a process known as Debye shielding (or screening), which modulates the electron beam density. Because these density modulations are going to be used in the rest of the CeC system, it is essential to understand the modulation process to get an accurate estimation of the cooling time. For an ion moving in an infinite, uniform electron distribution, an analytical solution of the modulation process was calculated in [21]. For a nonuniform electron distribution, different numerical approaches were carried out, such as in [22–25]. These numerical methods were benchmarked with the analytical solution of the uniform electron beam without external fields. Although density modulations of the electron beam were observed in 2020 [26], we have not found in the literature any benchmarking of these simulations with the experiments.

The underlying physical mechanism of many plasma phenomena, such as Debye shielding, is directly related to collisions, and hence an  $N$ -body approach is crucial [27]. Therefore, we performed simulations of the modulation process using our collisional method, particles' high-order adaptive dynamics (PHAD) [28]. PHAD capabilities of simulating complicated beam dynamics were demonstrated and benchmarked with experiments in [28–30]. A critical feature of PHAD is that it can deal with any particle distributions and easily include realistic external fields along the beamline. This is an important feature for simulating the modulator that consists of a set of four focusing quadrupoles and a non-uniform beam distribution. In addition, PHAD simulations naturally include all the collective effects due to the multi-species collisional interactions.

In this paper, we present our PHAD simulations of the modulator section of the CeC PoP experiments, aiming to quantify the best initial configuration of the ion beam that can give strong density modulations of the electron beam, and examine some cooling limitations and the limitations of other simulation methods. Our preliminary results were presented in [28,29]. The organization of the paper is as follows: A short overview of the CeC PoP experiments and the modulator section, along with our simulation method PHAD are described in Sec. II; the simulation details and results are presented in Sec. III, followed by analysis and

discussion in Section IV; we conclude with a brief summary in Sec. V.

## II. THE SETUP

Any implementation of the CeC system operates as follows: In the modulator, the cooling electrons co-propagate with the ions at the same velocity and the electron density gets modulated by the ions; then these density modulations are amplified in the amplifier section; in the kicker, the amplified modulated electron density is fed back to the ions to receive energy kicks toward their central energy. As a result, the ion beam's longitudinal emittance and energy spread are reduced, and the beam is cooled.

In early 2020, BNL was selected by the U.S. Department of Energy to be the site of the EIC that is being constructed currently by modifying the existing RHIC [1]. In order to test the CeC concept before it can be applied to achieve high luminosity in EIC, PoP experiments were proposed in [20], and the CeC accelerator was commissioned in the past years during RHIC 2015–2018 runs. In RHIC 2018 run, cooling was not observed by the FEL-based CeC experiment mainly due to unexpected strong noise in the electron beam, and thus density modulations were not observed [19]. Investigation of the cause of this excessive noise entailed the discovery of a new type of instability that was termed the plasma-cascade instability (PCI) [19]. In RHIC 2019–2020 runs, the PCI was systematically studied and led to the proposal of using the PCI as an amplifier in the CeC scheme [26,31]. With this plasma-cascade amplifier (PCA), the PCA-based CeC experiment was commissioned, where the density modulations of the electron beam were observed, and a high gain amplification with the PCA was demonstrated [26]. In the following runs, the CeC experiments continued with more improvements, as they met other challenges and difficulties; CeC is yet to be demonstrated [32].

### A. Modulator section of the CeC experiment

The PoP experiments at RHIC are described in [25], where the modulator section was 3 m long and included four quadrupoles each of length 0.157 m, separated by equal drift space of  $\sim 0.4$  m. The magnetic field gradients of the quadrupoles are 0.5528,  $-0.6220$ ,  $-0.0511$ , and 0.6072 T/m, where the first and last quadrupoles are focusing and the two middle quadrupoles are defocusing. In these experiments, the electron beam charge was 1 nC with a peak current of 100 A, full bunch length of 10 ps, and  $10^{-3}$  relative rms energy spread. Its distribution was Gaussian with rms normalized emittance 5 mm mrad, and  $\beta_{x,y} = 4.2$  m and  $\alpha_{x,y} = 0$  at the entrance. In the lab frame, the electrons' plasma frequency is  $1.5 \times 10^8$  rad/s, and the transverse and longitudinal Debye lengths are 0.34 mm and 1.1  $\mu\text{m}$ , respectively. The transverse size of the initially axisymmetric electron beam varies along this lattice, where

the horizontal beam size reaches a minimum and the vertical beam size reaches a maximum after the second quadrupole. For the ion beam, the ions are fully stripped gold ions  $\text{Au}^{79+}$ , with bunch intensity of  $10^9$  and rms bunch length of 60 cm. The design energy for both beams corresponds to  $\gamma = 42.9$  so that the velocity of the electron beam is matched by that of the ion beam.

## B. Simulation method

Coherent electron cooling, although it belongs to the family of stochastic cooling methods, shares similarities with electron cooling as they both use electrons to cool the hadron beams. It is well known that the simulation of electron cooling of heavy ions is one of the most challenging problems in computational beam dynamics. That is due to the vast length and time scales of the problem, involving a huge number of particles, and the end goal of extracting small quantities that are easily swamped by numerical artifacts of the underlying algorithms. Hence, the most electron cooling codes are phenomenological or macroscopic, using effective theories based on friction force [9,33–37]. While there are first-principle simulations based on direct numerical modeling of binary collisions to evaluate the friction force and the diffusion coefficient with a known degree of accuracy such as in [38], first-principle simulations in terms of solving the equations of motion of

TABLE I. Parameters used for the simulations of the modulator section of the CeC. See [28] for the meaning of PHAD parameters; these were selected as optimum for high prescribed accuracy.

Parameter (unit)	Value
$\gamma$	42.9
Number of electrons	$10^5$
Electron beam rms $\sigma_{x,y}$ (mm)	0.12
Electron beam $\varepsilon_{x,y}$ (mm mrad)	0.003
Electron beam rms $\sigma_z$ ( $\mu\text{m}$ )	1.1
Electron beam $\Delta p/p$	$10^{-5}$
Modulator length (m)	3
Drift before first quadrupole (m)	0.4245
Drift between quadrupoles (m)	0.393
Quadrupoles lengths (m)	0.157
First quadrupole strength (T/m)	0.5528
Second quadrupole strength (T/m)	-0.6220
Third quadrupole strength (T/m)	-0.0511
Fourth quadrupole strength (T/m)	0.6072
PHAD timestep (ps)	$\sim 16.7$
Number of PHAD timesteps	600
Clustering parameter $q$	60
FMM order	6
Accuracy	$10^{-9}$
Simò maximum order	10
Type of time bins	Equal widths
Number of time bins	10

the particles derived from Coulomb force and Lorentz force while considering the discrete nature of the  $N$  particles, i.e., as an  $N$ -body problem were not realized until recently by our previous work. Our group is the only one to employ first principles, microscopic algorithms packaged into an efficient parallelized framework, PHAD [28], which allowed the first benchmarked simulations of conventional, bunched, low-energy electron cooling [30].

Realistic, high-fidelity simulations are enabled by the combination of accurate and efficient computation of pairwise particle interactions, including the stochastic part of Coulomb interactions, by the fast multipole method (FMM) [39]; the provably optimal propagation of each particle in time using a novel (Simò) integrator with *a priori* set accuracy, capable of resolving even the closest close encounters [40]; a splitting scheme to preserve symplecticity of long-term simulations to machine precision [41]; and extensive parallelization, enabling running the software on large-scale, distributed hardware compute clusters. The FMM technique naturally provides rigorous error bounds, and our implementation of the multilevel FMM enables efficient error control [39]. Thus, the numerical noise/errors are negligible due to our ability to set error tolerances *a priori* close to the machine precision. For more details regarding PHAD and its constitutive algorithms, we refer the reader to [28].

Clearly, PHAD is also well suited to coherent electron cooling simulations, especially of the modulator sections. In fact, since the high accuracy and efficiency of the algorithms are maintained and translated without change from conventional to coherent electron cooling, the relatively short time scale of the modulation allows realistic

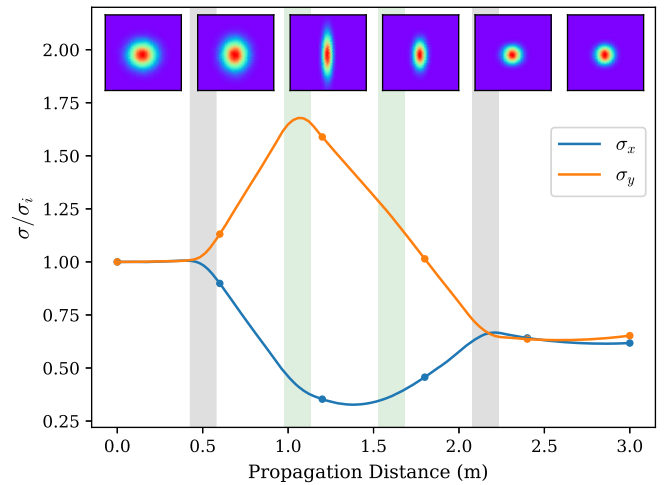


FIG. 1. Effect of the modulator lattice of the CeC on the transverse dynamics of the electron beam as simulated by PHAD showing the evolution of the transverse size normalized to the initial size. The solid points show where the transverse densities are plotted in the top insets. The shaded areas represent the positions of the quadrupoles where gray is for focusing and green is for defocusing.

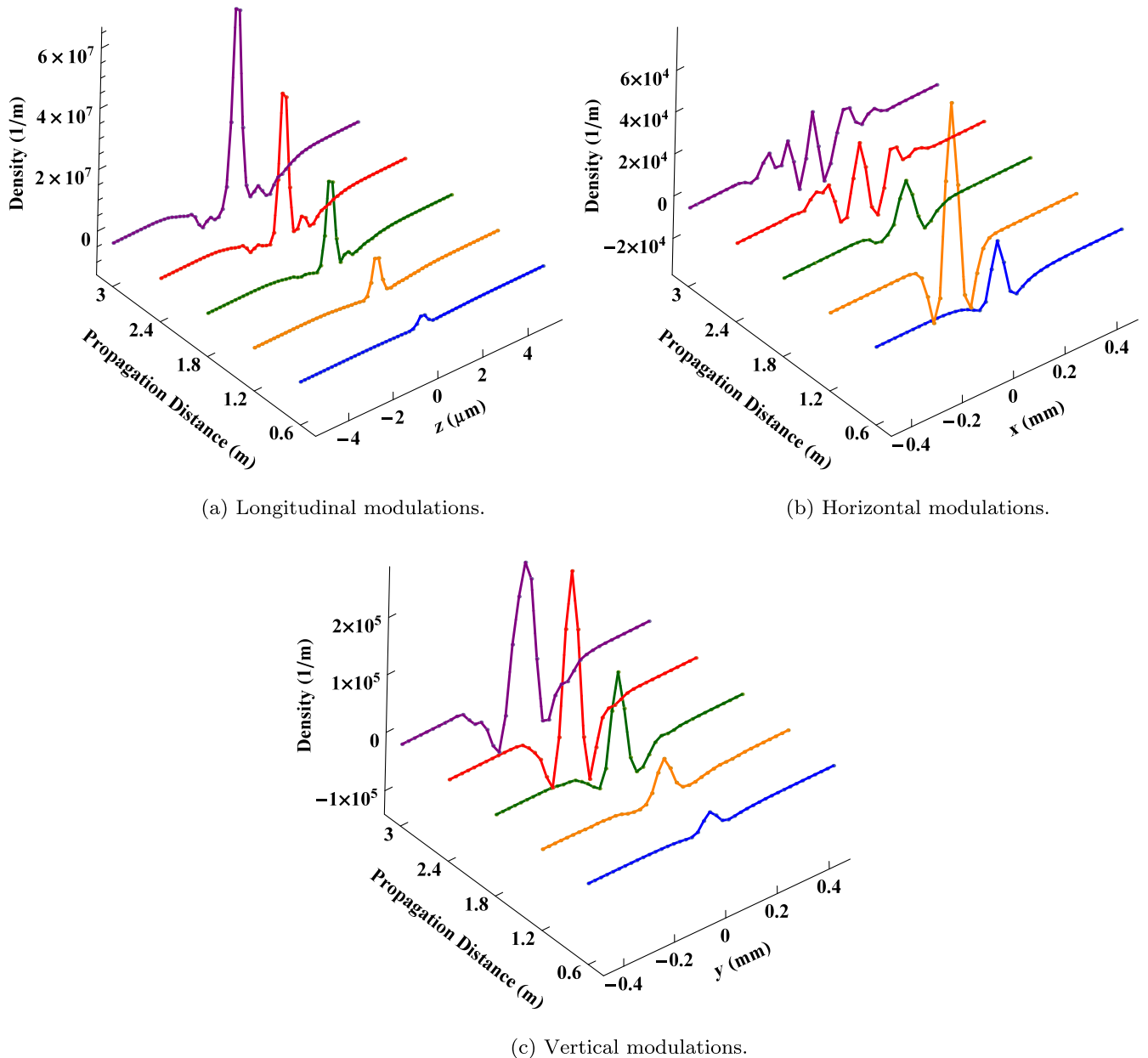


FIG. 2. PHAD simulations of density modulations of the electron beam due to a single centered ion through the modulator section of the PoP CeC at RHIC. The longitudinal signal increases with the propagation distance while the transverse density varies according to the modulator lattice.

scans of the parameter space with unprecedented detail. Indeed, in addition to getting insight into the modulation physics and optimization of system parameters, we also keep an eye on similarities and differences in the outcomes between our approach and the more traditional, macroscopic approaches, made possible by PHAD. Although PHAD is more than capable of running electron cooling simulations with a large number of ions (as in [30]), the main topics addressed here make sense only with one or few ions. Otherwise, maximizing density perturbations, evaluating ultimate cooling performance, or establishing some limitations of the superposition principle would be

more difficult to discern. Future work will address full-scale, high-fidelity simulations.

Here our main goal is to quantify the best initial configurations of the ion beams that can give strong density modulations to the electron beams and examine some cooling limitations. As explained by [25], particle simulations result in a shot noise much larger than the density modulations, which makes it difficult to observe the modulation signal. To extract the signal, we apply two procedures. The first one follows the method used by [25], where two simulations are performed with the same electron distribution, but one of them includes the ions

and the other is without the ions. Throughout the modulator section, the two resulting electron distributions are subtracted to extract the modulation signal. The second procedure is to apply signal averaging, where we perform many simulations with new random number seeding of the electrons' positions and momenta of the same initial condition distributions and take the average of the results of these simulations. We choose to use the first approach in all our simulations of various configurations because it gives a much clearer signal that is easier to quantify and interpret. To compare the two approaches, we illustrate it with one simulation utilizing the second approach.

It is worth noting that the shot noise in particle simulations is different from the excessive noise in the electron beam detected in early CeC experiments at RHIC. While both obstruct the observation of the modulation signal, their origins are different. The shot noise in the simulations is due to the random generation of the nonuniform space and thermal motion distributions. As the electrons interact with the ions, the resulting modulation signal due to their physical redistribution is orders of magnitude smaller than the shot noise. On the other hand, the noise in the early experiments was due to an unexpected instability that occurs in beams propagating in straight sections. The CeC team at RHIC discovered that instability and called it as plasma-cascade instability (PCI) [19]. They studied in detail the PCI and they were able to observe density modulations in later CeC experiments [26,31].

### III. SIMULATIONS AND RESULTS

Since the size of the electron beams in the PoP CeC experiments at RHIC described in [25] are large compared to the lengths related to the ion's shielding (Debye lengths), and because the far away electrons do not contribute to the shielding, we consider only a small part of the beam. Because the longitudinal Debye length is much smaller than the transverse one, we consider a longitudinal slice of the electron beam with a relatively smaller transverse size than the one in the experiments. This slice is large enough that it does not require applying periodic boundary conditions to counteract the dynamic expansion of the concentrated electron beam slice. We demonstrate this in Sec. III A where we show that extending the electron beam size does not influence the results.

The modulator simulations were performed by PHAD for  $\text{Au}^{79+}$  ions of zero transverse momenta, and we used a Gaussian distributed electron beam with the parameters described in Table I along with PHAD parameters. The parameters in Table I were applied in all subsequent simulations unless otherwise noted.

Before we present density modulation results, we propagated an electron beam through the modulator to observe the effect of the quadrupoles on its transverse size. The evolution of the transverse size is illustrated in Fig. 1 where the horizontal beam size (blue curve) starts

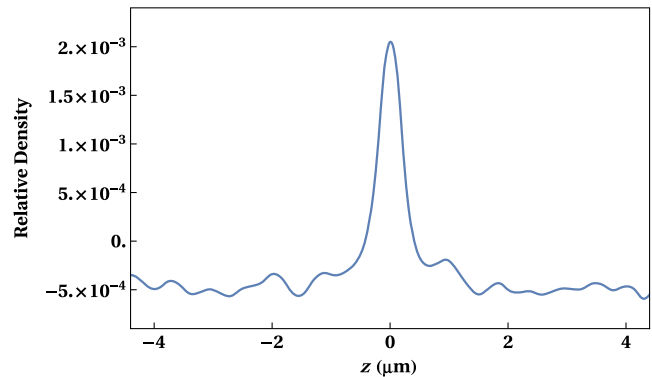


FIG. 3. Relative longitudinal density modulation due to a centered ion at the end of the modulator section of the CeC from PHAD simulations.

decreasing after the first quadrupole at 0.6 m, reaches a minimum after the second quadrupole at 1.2 m, and increases after that. The vertical beam size (orange curve) behaves in the opposite way and reaches a maximum after the second quadrupole at 1.2 m. These changes are also shown through the density plots of the transverse beam size at different propagation distances along the modulator section depicted in the top insets of Fig. 1. Therefore, we expect the density modulations due to the ions to be affected by these changes of the transverse beam size along the modulator. Because of the Gaussian distribution of the electrons, this variation of the beam size would influence the strength of the modulation signal for off-axis ions transversely, where the number of electrons around them will vary as well.

#### A. Simulations with a single ion

We start with a single ion at the center of the electron beam and we extract the modulation signal along the modulator section. Then, we study the effect of varying the location of the ion and its momentum with respect to the

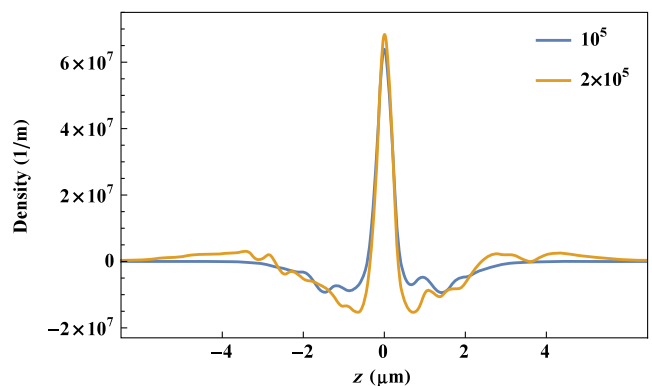


FIG. 4. Comparison of longitudinal density modulations from two simulations of the same density, but different size and number of electrons. One simulation included  $10^5$  electrons within  $\sigma_z$ , and the other included  $2 \times 10^5$  electrons within  $2\sigma_z$  of the same density.

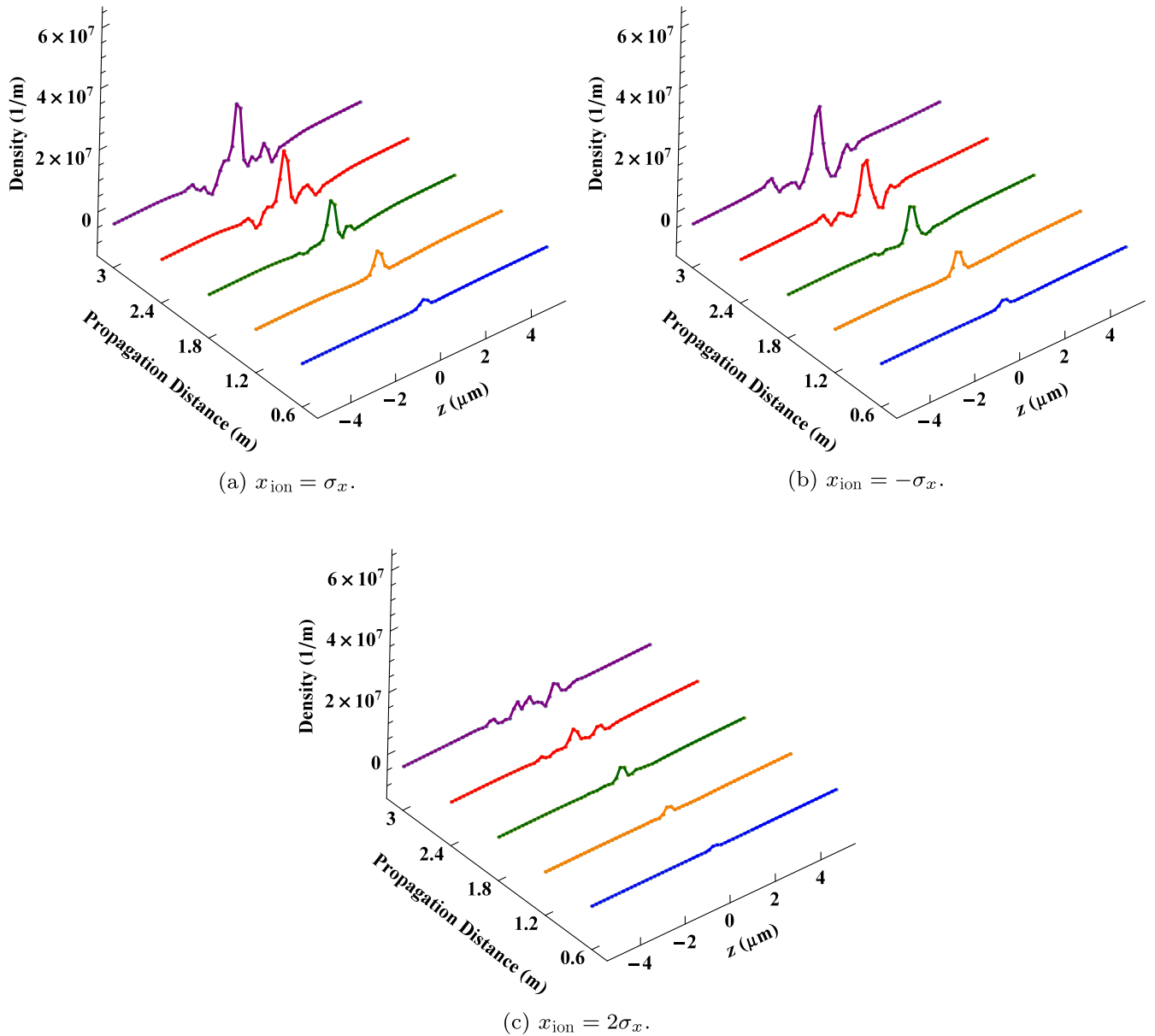


FIG. 5. PHAD simulations of the longitudinal density modulations of electron beams through the modulator section of the PoP CeC at RHIC with a single ion located at  $(x_{\text{ion}}, 0, 0)$  for different  $x_{\text{ion}}$ . The signal is reduced by the displacement from the center of  $x$  axis compared to the centered ion.

electron beam reference frame. Figure 2 shows the density modulations of the electron beam due to a centered ion. In the longitudinal direction, the signal increases with the propagation distance while the evolution of the transverse modulations reflects the effect of the modulator quadrupoles on the transverse beam size. The horizontal modulation signal reaches the maximum when the horizontal beam size is minimum at 1.2 m. For the vertical modulations, the vertical beam size is minimum at about 2.4 m, where the signal is maximized. Note that in all of our plots of the density modulation signal, the vertical axis could be negative since this signal is a result of the subtraction of two densities. This is not a negative density and it means that

there are less electrons in this region in the simulation with ions compared to the simulation without ions, which is a result of shielding the ions.

Because only the longitudinal modulations are related directly to the concept of the CeC, we will mostly present the results of the density modulations in the longitudinal direction in the remaining simulations. The relative longitudinal density modulation for the case of the centered ion is small and is on the order of  $10^{-3}$  at the end of the modulator section as shown in Fig. 3.

Before we continue with different ion configurations, we show that our choice of simulating a longitudinal slice gives results similar to the one by a larger beam of the

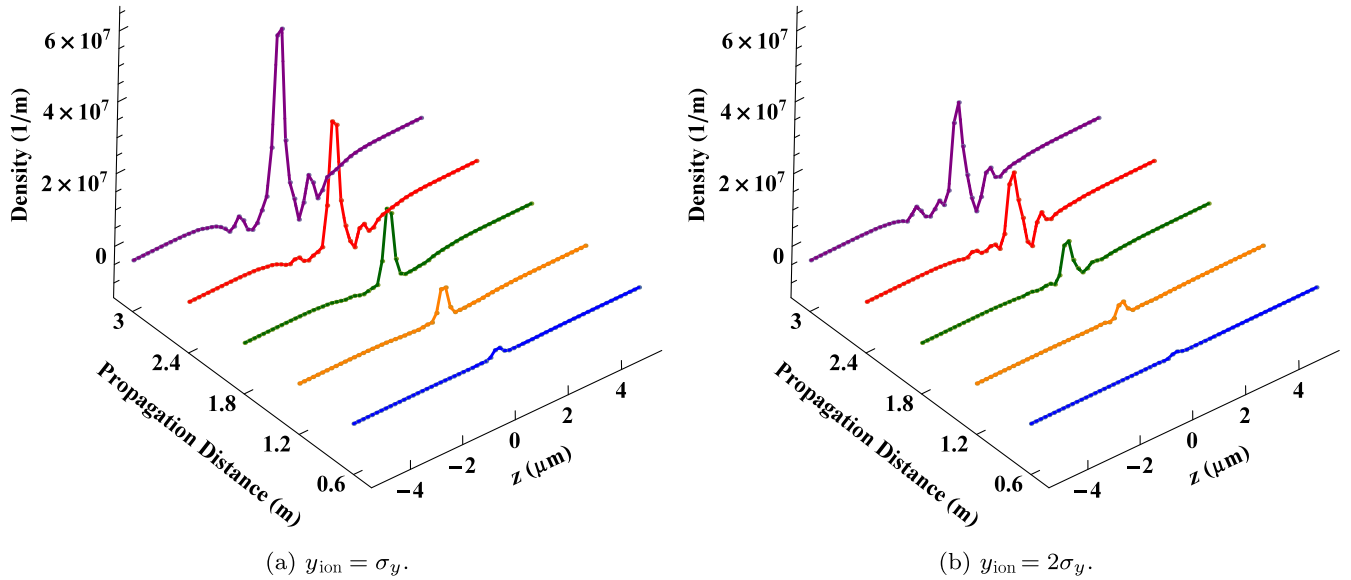


FIG. 6. PHAD simulations of the longitudinal density modulations of the electron beams through the modulator section of the PoP CeC at RHIC with a single ion located at  $(0, y_{\text{ion}}, 0)$  for: (a)  $y_{\text{ion}} = \sigma_y$  and (b)  $y_{\text{ion}} = 2\sigma_y$ . The signal decreases as the ion displacement from the center increases.

same density. Thus we increase both the longitudinal beam size and the number of electrons by a factor of two and compare its results with the previous results. In this case, the larger beam has  $2 \times 10^5$  electrons and its longitudinal rms size is  $2\sigma_z$ . The results are shown in Fig. 4, where the resulting longitudinal density modulations are almost identical. This also shows that our choice of the electron slice is large enough that the edge effects can be neglected. Hence there is no need for periodic boundary conditions as the case for a thin slice.

Now, we consider an off-axis ion with respect to the center of the electron beam. Let the position of the ion be at  $(x_{\text{ion}}, 0, 0)$ , and we vary  $x_{\text{ion}}$  as  $\pm\sigma_x$  and  $2\sigma_x$ . The results are

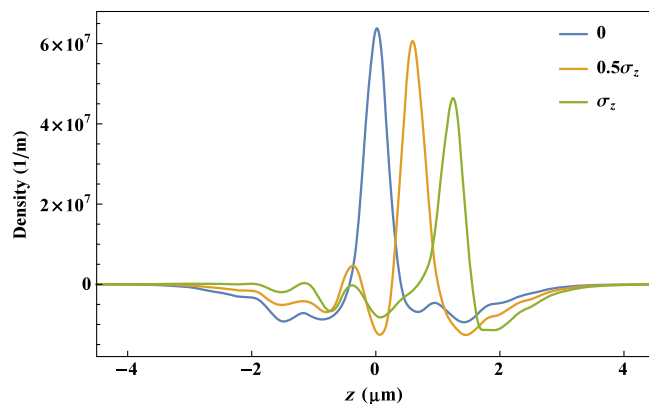


FIG. 7. Comparison between the longitudinal density modulations of  $10^5$  electrons for an ion located at  $(0, 0, z_{\text{ion}})$  when  $z_{\text{ion}} = 0, 0.5\sigma_z$ , and  $\sigma_z$ . The reduction of the signal due to off-centered ions is a result of the decrease in the number of electrons.

shown in Fig. 5, where the decline of the signal compared to the centered ion is clear. The longitudinal signal is about the same for  $x_{\text{ion}} = \pm\sigma_x$ , and it decreases as the distance from the  $x$ -axis center increases as for the  $x_{\text{ion}} = 2\sigma_x$  case. The reason for this decrease is the Gaussian distribution of the electrons, where the number of electrons around the ion decreases the further the ion is displaced from the  $x$ -axis center, and it almost disappears for distances more than  $\sigma_x$ .

Since the effect of the modulator lattice on the transverse size of the electron beam differs between the horizontal and the vertical, we also consider an ion off center on the  $y$  axis by  $\sigma_y$  and  $2\sigma_y$ . The resulting longitudinal density modulations along the modulator section are shown in Fig. 6. Compared to the signal of the centered ion, the signal decreases for the ion at  $\sigma_y$  and decreases more at  $2\sigma_y$ , reflecting the lower number of electrons further away from the electron beam core. We also notice that the longitudinal signal is less affected by displacing the ion along the  $y$  axis compared to the displacement of the ion along the  $x$  axis by the same amount. The reason for that is that the vertical size of the electron beam is larger than the horizontal size and the ion sees more electrons throughout most of the modulator.

Although a longitudinal slice of the electron beam can be reasonably represented by a uniform distribution longitudinally, we chose a Gaussian distribution to show the effect of the ion placed off core of the electron beam. Accordingly, we consider an ion to be off center along the  $z$  axis by about  $0.5\sigma_z$  and then by  $\sigma_z$ . We compare the ensuing modulation signals with the one from the centered ion as shown in Fig. 7, where it can be seen that the signal decreases as we move away from the center of the electron

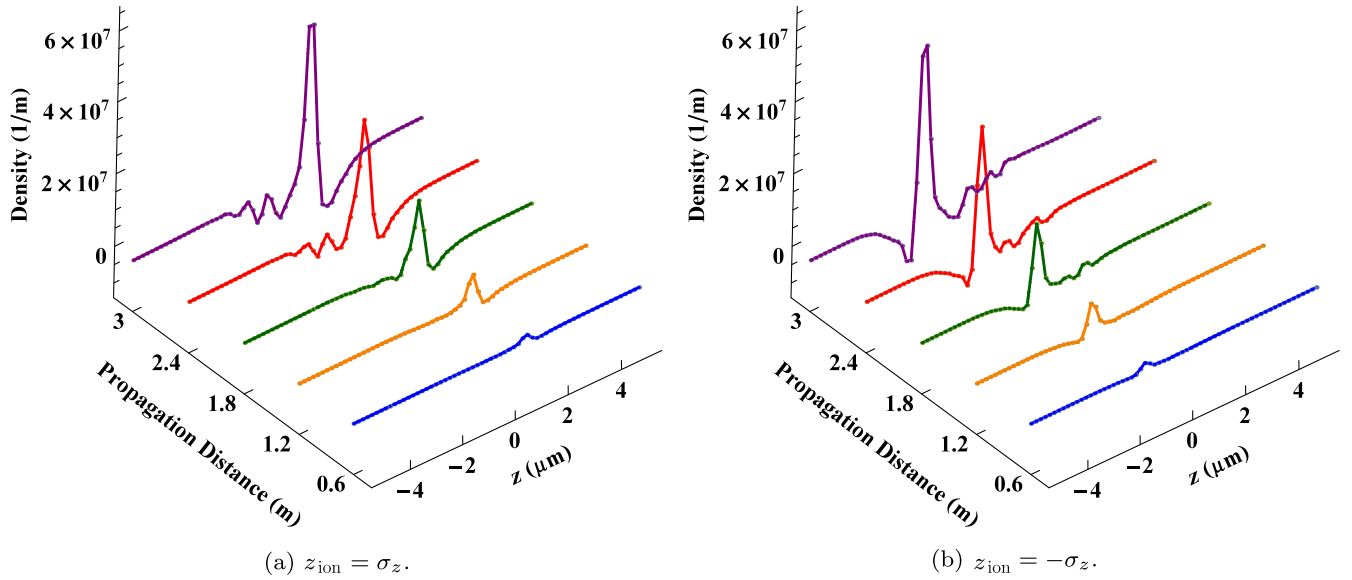


FIG. 8. PHAD simulations of the longitudinal density modulations of the electron beam through the modulator section of the PoP CeC at RHIC with a single ion located at  $(0, 0, z_{\text{ion}})$  for  $z_{\text{ion}} = \pm\sigma_z$ . The signals are displaced to the location of the ions and are of the same strength.

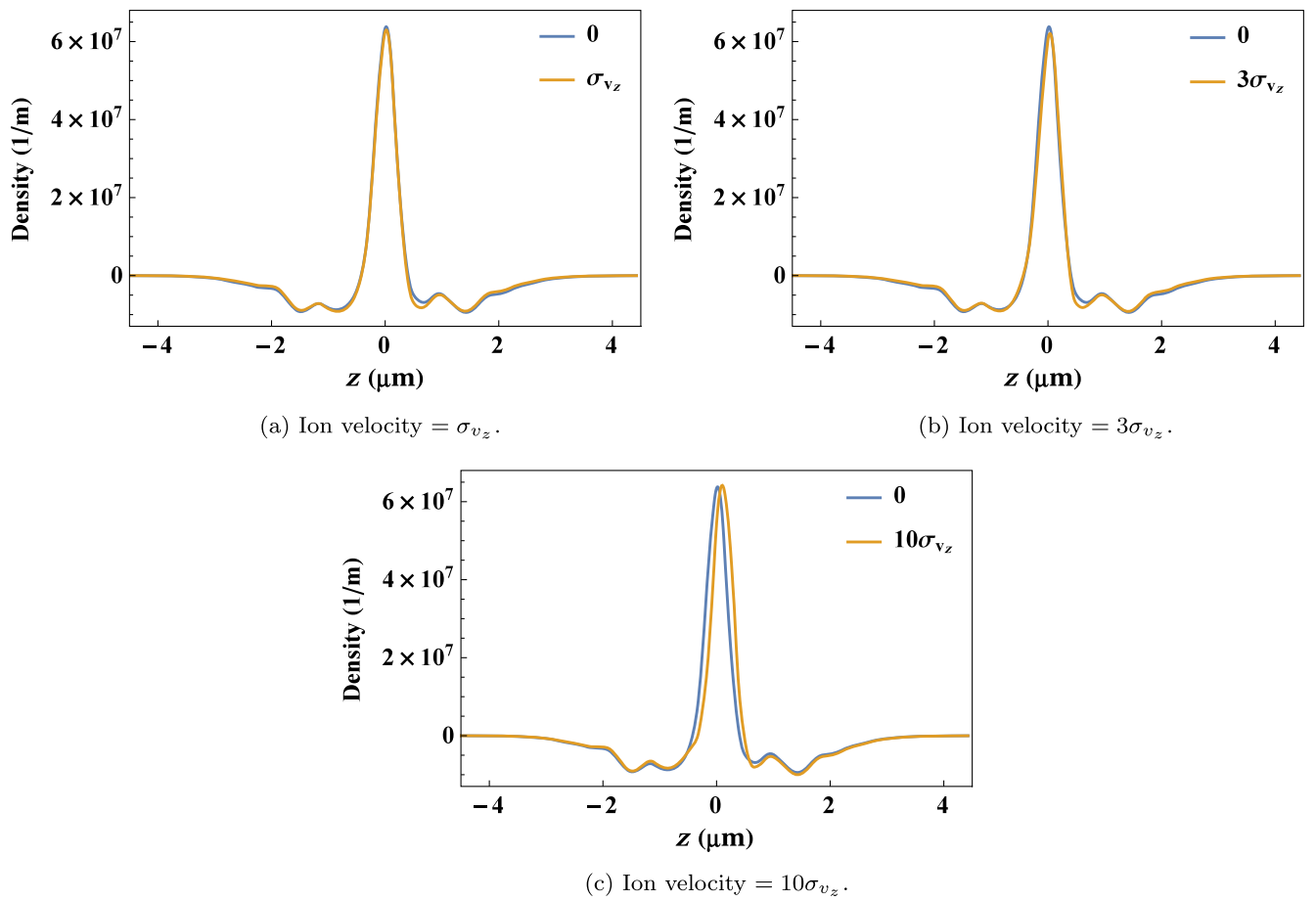
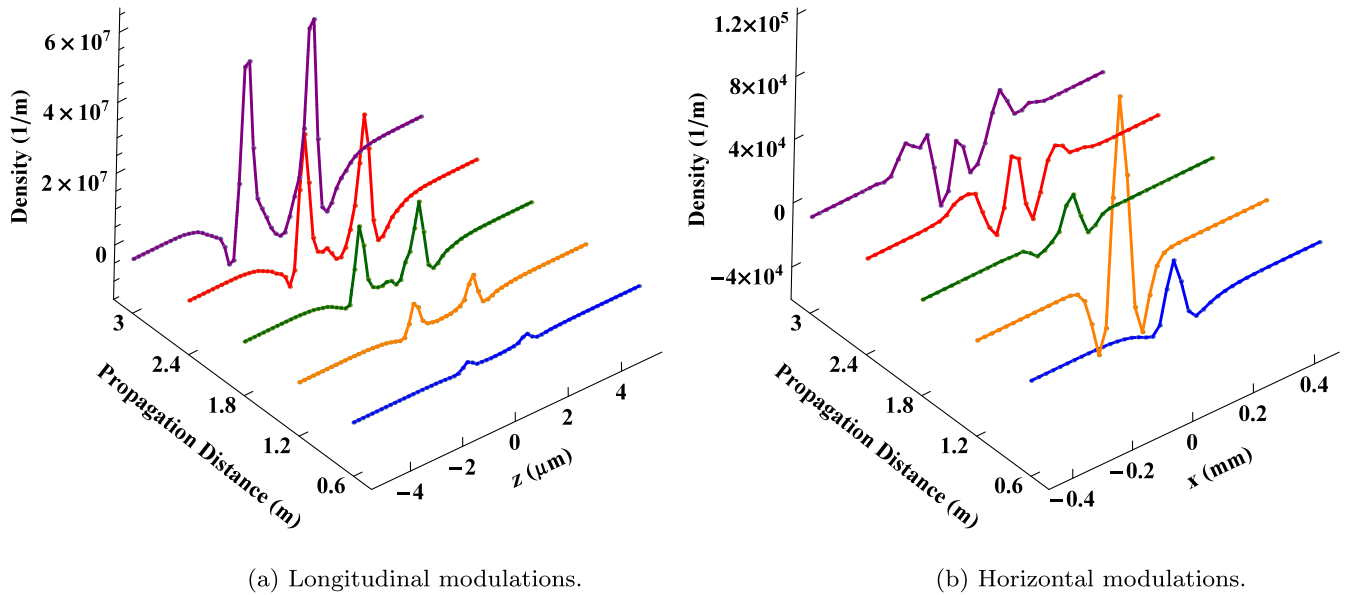
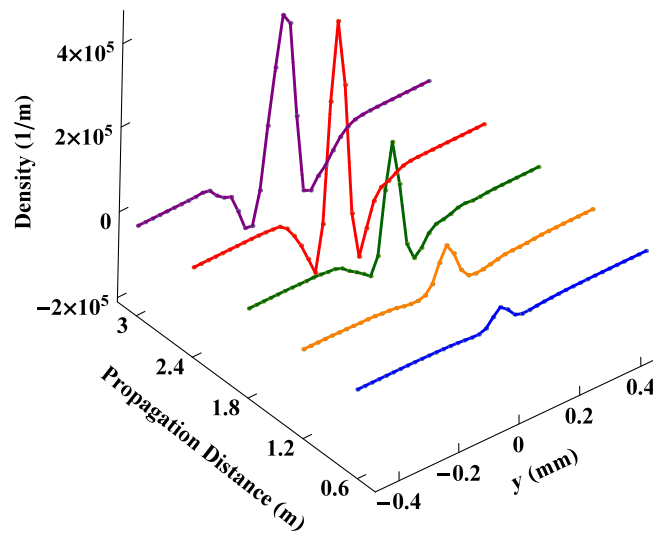


FIG. 9. PHAD simulations of the longitudinal density modulations of the electron beam due to a centered ion, moving with respect to the electron beam through the modulator section of the PoP CeC at RHIC. The signal due to the moving ion is compared to that of the stationary ion for ion's velocities: (a)  $\sigma_{v_z}$ , (b)  $3\sigma_{v_z}$ , and (c)  $10\sigma_{v_z}$ .



(a) Longitudinal modulations.

(b) Horizontal modulations.



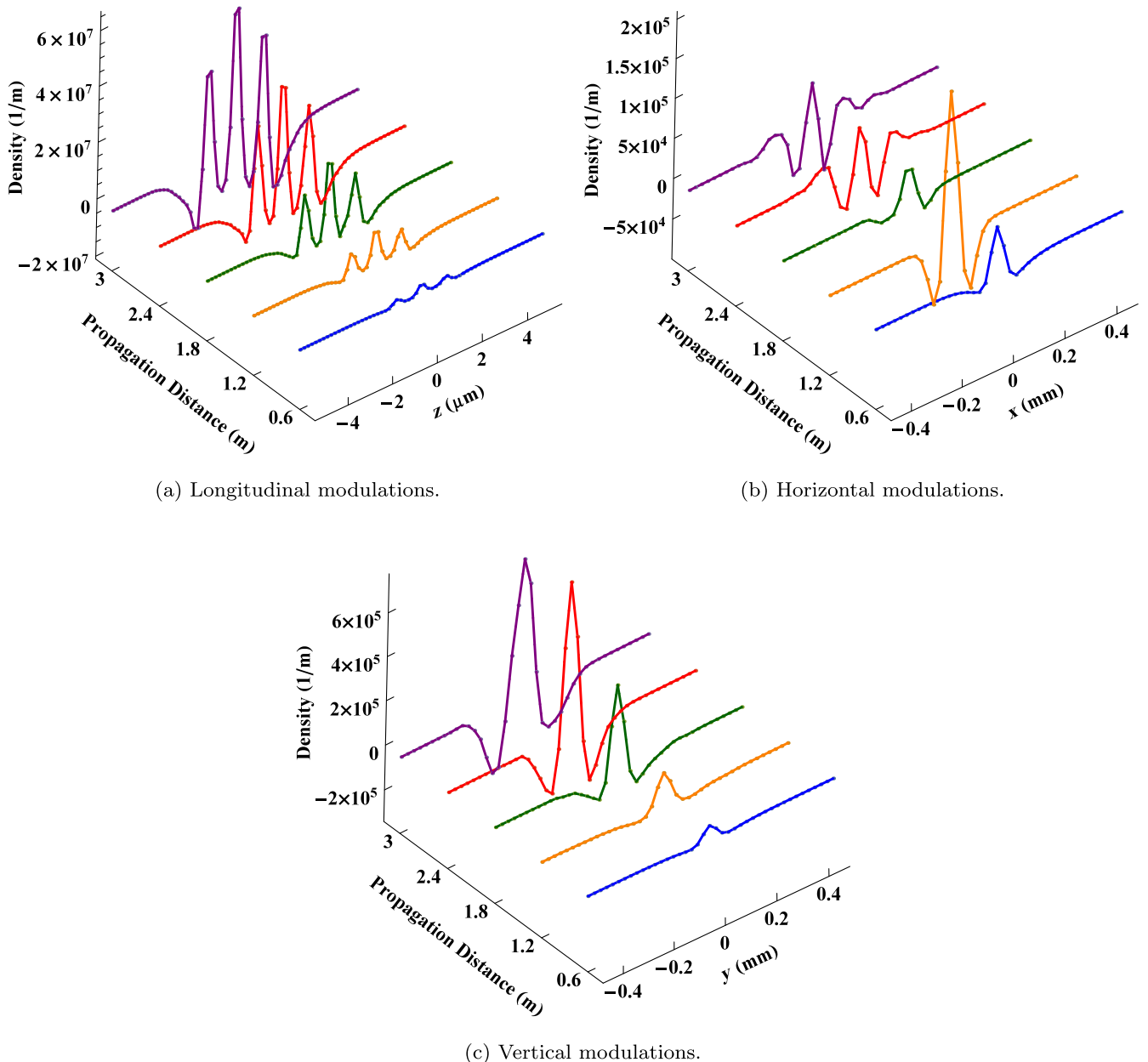
(c) Vertical modulations.

FIG. 10. PHAD simulations of density modulations of the electron beam through the modulator section of the PoP CeC at RHIC due to two ions, one is at  $\sigma_z$  and the other is at  $-\sigma_z$ . There are two peaks around the two ions longitudinally, and the signal is about twice that of a single ion transversely.

beam. The decreased signal reflects the decrease in the number of electrons away from the core of the electron beam. If we compare the signal due to the ion at  $\sigma_z$  with the one due to the ion at  $-\sigma_z$ , both off the  $z$  axis, we see in Fig. 8 that the strength of both signals is the same which is due to the symmetry of the electron beam longitudinally.

Going back to an ion at  $(0, 0, 0)$ , we vary the ion's velocity with respect to the electron beam velocity. In the frame of the electron beam, the velocity spread of the electron beam is  $\sigma_{v_z}$ . We start with an ion moving with a velocity of  $\sigma_{v_z}$  and  $3\sigma_{v_z}$  with respect to the electron beam.

Because the electrons' velocity spread in the CeC experiments is much larger than the one we used in our simulations, we also simulated a moving ion with a velocity of  $10\sigma_{v_z}$  with respect to the electron beam. The results are shown in Fig. 9 and compared to a stationary ion with respect to the electron beam. For the  $\sigma_{v_z}$  ion, there is almost no change in the signal while there is a small change for the  $3\sigma_{v_z}$  ion, also becoming slightly asymmetric. The asymmetry is clear for the  $10\sigma_{v_z}$  ion with a small displacement as the ion itself has moved ahead from the center of the electron beam.



(a) Longitudinal modulations.

(b) Horizontal modulations.

(c) Vertical modulations.

FIG. 11. PHAD simulations of density modulations of the electron beam through the modulator section of the PoP CeC at RHIC due to three ions placed at  $-\sigma_z$ ,  $0$ , and  $\sigma_z$ . There are three peaks around the three ions longitudinally, and the signal is about 3 times that of a single ion transversely.

### B. Simulations with multiple ions

We performed simulations that include more than one ion at different locations longitudinally and propagated them surrounded by the electron beam through the modulator section. First, we considered two ions, in which one ion is positioned at  $(0, 0, \sigma_z)$  and the other is at  $(0, 0, -\sigma_z)$ , and extracted the modulation signal. In Fig. 10, there are two peaks around the positions of both ions in the longitudinal direction, and the strength of the signal in the transverse direction is about twice that of one ion. Then we add one more ion at the center of the electron beam

$(0, 0, 0)$  and get the density modulations due to the three ions in Fig. 11. Similar to the two ions' case, there are three peaks around the positions of the ions longitudinally, and the strength of the signal in the transverse direction is about 3 times that due to one ion.

The variation of the strength of the longitudinal signal around the three ions in Fig. 11(a) reflects the Gaussian distribution of the electrons. When the longitudinal distribution of the electrons is uniform, the three signals should be the same. We show that this is the case with a uniform longitudinal electron distribution of length  $4\sigma_z$  in Fig. 12.

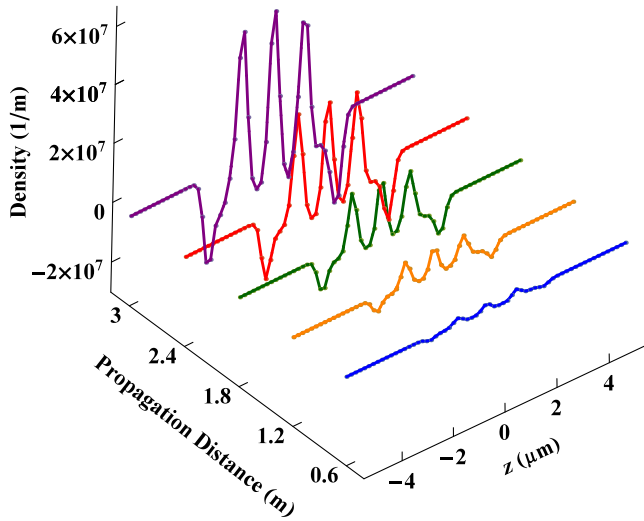
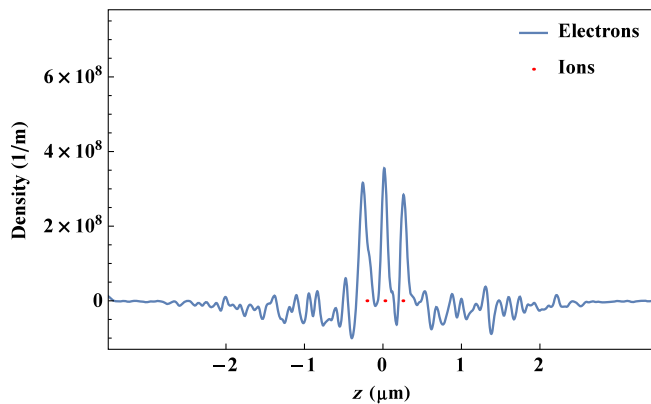
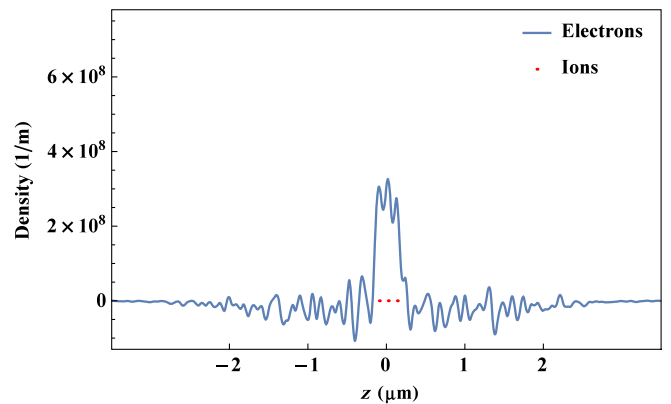


FIG. 12. Longitudinal modulation signals due to three ions in a uniform longitudinal electron distribution showing that the strengths of the signals are the same compared to the case of the Gaussian distribution where the strengths vary.

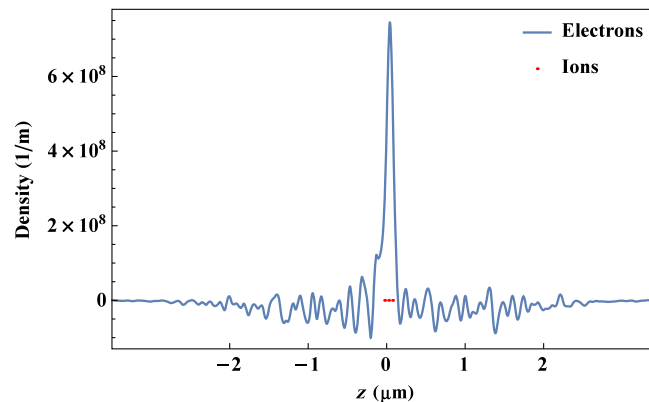
The simulations presented in this section show clear signals around the ions' locations when placed about  $d = \sigma_z$  apart longitudinally. This leads to the following question: how would the signals be affected if the ions were much closer to each other? The expectation is that, at some point, the electrons would see the ions as one with a higher charge and there will be one peak around those ions. To get an estimation of the distance between the ions that this would happen (the “resolution”), we performed simulations varying  $d$  between three ions. Figure 13 shows our results for  $d = 0.2, 0.1,$  and  $0.05 \mu\text{m}$  at the end of the modulator section. For  $d = 0.2 \mu\text{m}$ , we can see three clear signals around the ions. The three signals start to become less well defined for  $d = 0.1 \mu\text{m}$ , and they become one large signal when  $d = 0.05 \mu\text{m}$ . This loss of resolution is not an artifact of the type and number of bins used in our simulations. Thus, it is possible to say that the density modulations are cleaner when the distance between the ions is larger than  $d = 0.1 \mu\text{m}$ . In fact, there is no need (in fact, it is impossible) for more cooling when the ions are as close to each other such that they cannot be distinguished anymore by the surrounding electrons.



(a) Distance between ions =  $0.2 \mu\text{m}$



(b) Distance between ions =  $0.1 \mu\text{m}$



(c) Distance between ions =  $0.05 \mu\text{m}$

FIG. 13. PHAD simulation results at the end of the modulator section showing density modulations of the electron beam due to three ions when the distance between the ions is (a)  $0.2 \mu\text{m}$ , (b)  $0.1 \mu\text{m}$ , and (c)  $0.05 \mu\text{m}$ . The modulation is improved when the ions are placed more than  $0.1 \mu\text{m}$  apart.

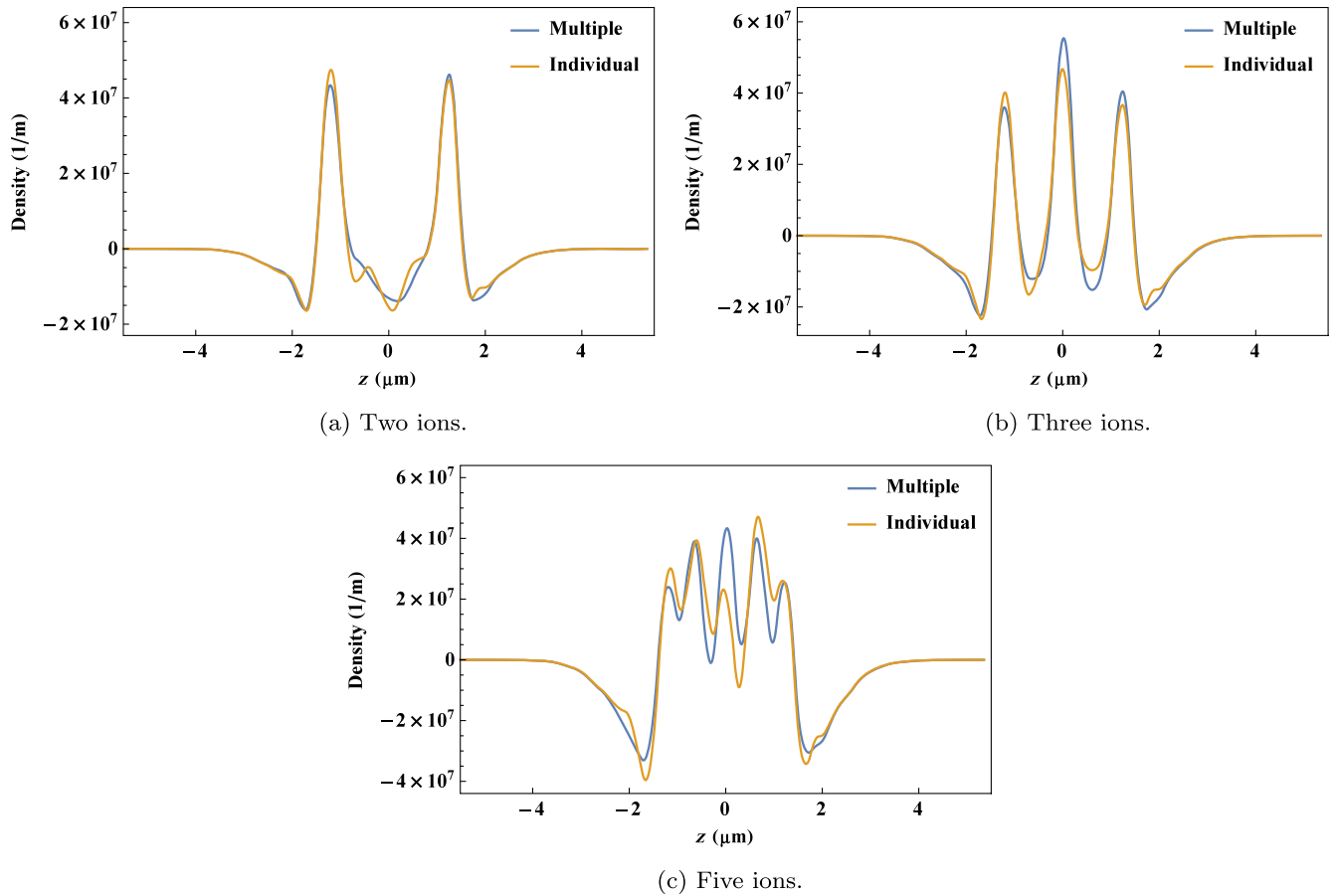


FIG. 14. Comparison between the modulation signals when the signal is a result of one simulation of multiple ions (blue) and when the signal is a superposition of signals due to individual ions (orange). The density modulations are due to (a) two ions, (b) three ions, and (c) five ions.

It was suggested in [42] that it is possible to perform simulations with a single ion in different configurations, extract the signal, and then apply the superposition principle to get the full effect of the ion beam on the electron beam. We have examined this proposition for three cases: two ions, three ions, and five ions. The ions were positioned on axis transversely, and longitudinally the two ions were positioned at  $\pm\sigma_z$  for the two ions case; a third ion was at the center of the axis for the three ions case; two additional ions were positioned at  $\pm 0.5\sigma_z$  for the five ions case. We show in Fig. 14, a comparison between the extracted signal when the simulations were performed with multiple ions (blue curve) and when the emerging signals were a superposition of each signal of individual ions separately (orange curve). For the two ions case in Fig. 14(a), the signals from both ways were almost the same. However, the signals started to differ when more ions were included. This difference is small for the three ions case in Fig. 14(b), and it is noticeably large for the five ions case in Fig. 14(c). As we added ions into the same density and bunch length of the electrons, the distance between the ions decreases. While electrons can move freely, relatively, to shield a

single ion, that is not the case in the presence of other ions' attracting forces. Thus our results suggest that the superposition principle should be used carefully, as it can give inaccurate signals when ions are close enough longitudinally. In addition, a uniform longitudinal distribution of the electron beam slice as used in [42] may improve the results of the superposition due to the fixed density. However, as the longitudinal position of the ion varies along the whole Gaussian electron beam, the electron density around it varies as well. These variations must be considered when applying the superposition principle.

### C. Signal averaging simulations with one ion

Using the same parameters from Table I and a single ion at the center of the electron beam, we performed 20 runs with differently seeded random generation of the electrons' positions and momenta. Then we performed signal averaging of the results where the signal tends to accumulate, and the noise is reduced. In Fig. 15, we show the results of the signal averaging at three different propagation distances, with an inset for the region where the signal should be. We see that the electron beam's longitudinal size increases

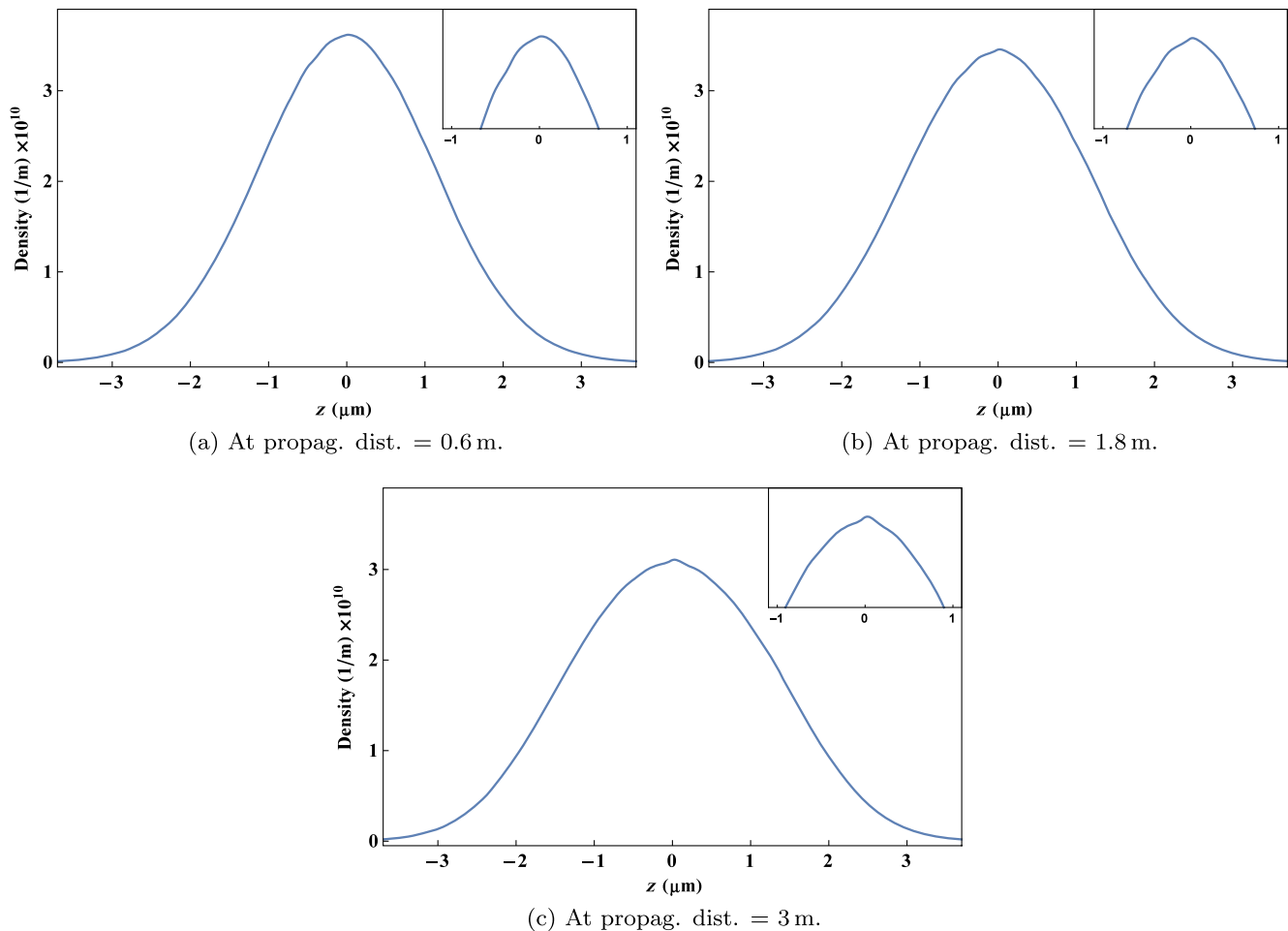


FIG. 15. PHAD simulations of density modulations of the electron beam due to a centered ion through the modulator section of the PoP CeC at RHIC, using signal averaging for 20 runs at different propagation distances: (a) 0.6 m, (b) 1.8 m, and (c) 3 m (end of the modulator section). The inset of each plot shows the region where the signal should be represented by the small centered bump in (b) and (c).

as it propagates through the modulator section and the signal becomes more visible toward the end. At 0.6 m, the signal is not visible indicating a weak signal, but it becomes clear (stronger) for propagation distances 1.8 m and the end of the modulator section at 3 m.

#### IV. DISCUSSION

In [24] and [25], simulations were performed with a larger beam size and density of the electrons than in our simulations. However, the behaviors of the density modulations for the centered, off axis transversely, and off-reference momentum ions are similar in both our simulations and in those references. The modulation signal due to a centered ion is the strongest and it starts to decrease as the ion is displaced off axis transversely reflecting the decrease in the number of electrons that can shield the ion and the focusing effects of the modulator lattice. An off-reference momentum ion results in a slightly smaller signal

with some asymmetry compared to the one due to the ion of reference momentum. Since PHAD simulations are based on first principles, our simulations support and verify the modulation simulation results in [24,25].

Our simulation results suggest that the best longitudinal density modulations due to the ions are achieved when the ions are well aligned with the center of the electron beam transversely and far from the electron beam edges longitudinally. Also, it is important to have a distance larger than 0.1 μm between the ions longitudinally to get a well-defined strong signal around each ion and thus achieve better cooling. When two ions are so close such that they are indistinguishable by the electron beam, which means no further cooling can be accomplished. One also has to be careful when using the superposition principle to combine the signals due to individual ions as that can become inaccurate if the variation of the electron density around each ion is not considered, especially when there are many ions in close proximity.

## V. SUMMARY AND CONCLUSIONS

We presented collisional simulations for the modulator section of the PoP experiment of the coherent electron cooling system in RHIC at BNL. These simulations were performed using the novel collisional nonlinear beam dynamics method PHAD, which is the first collisional method in beam physics. PHAD collisional simulations of the density modulations in the modulator section provide the most accurate description of this Debye shielding process of the ion by the surrounding electrons, which is a result of Coulomb collisions. Our results support the possibility of obtaining modulation signals and show that better signals, and thus better cooling, are achieved when the ions are on axis transversely. Longitudinally, the ions have to be within the core of the electron beam and without large variations of their velocities with respect to the electron beam (although not very sensitively). Modeling the multiple ions suggests that these ions have to be well separated (longitudinally) in order to obtain a clear, well-defined signal. If the ions are very close such that they are indistinguishable from the electron cloud, they cannot be cooled any further. This observation can suggest practical stopping mechanisms to avoid detrimental overcooling effects. Moreover, we showed that the superposition principle has to be applied carefully in combining signals due to individual ions, as it might lead to incorrect insights and misunderstandings when ions are close enough, especially when the longitudinal electron density is not uniform. Although we have shown that it is possible to extract the modulation signal using statistical averaging, the signals are very small with respect to the fluctuations in the electron distributions, and it is much more straightforward to quantify the modulations using the other approach of density subtraction, one with ions and one without.

## ACKNOWLEDGMENTS

This work was supported in part by the U.S. Department of Energy, Office of Nuclear Physics under Contract No. DE-SC0008588. This work used resources from the Center for Research Computing and Data at the Northern Illinois University.

- 
- [1] F. Willeke and J. Beebe-Wang, Electron ion collider conceptual design report 2021, Brookhaven National Laboratory (BNL), Upton, NY; Thomas Jefferson National Accelerator Facility (TJNAF), Newport News, VA, Technical Report No. BNL-221006-2021-FORE, 2021.
  - [2] Y. S. Derbenev, On possibilities of fast cooling of heavy particle beams, *AIP Conf. Proc.* **253**, 103 (1992).
  - [3] G. I. Budker, An effective method of damping particle oscillations in proton and antiproton storage rings, *Sov. At. Energy* **22**, 438 (1967).

- [4] G. I. Budker, N. S. Dikanskij, D. V. Pestrikov, I. N. Meshkov, V. I. Kudelainen, B. N. Sukhina, V. V. Parkhomchuk, and A. N. Skrinsky, Experimental studies of electron cooling, *Part. Accel.* **7**, 197 (1976), <https://cds.cern.ch/record/1021068/files/p197.pdf>.
- [5] S. van der Meer, Stochastic damping of betatron oscillations in the ISR, CERN, Geneva, Technical Report No. CERN-ISR-PO-72-31, 1972.
- [6] S. van der Meer, Stochastic cooling and the accumulation of antiprotons, *Rev. Mod. Phys.* **57**, 689 (1985).
- [7] E. Wang, S. Benson, W. Bergan, K. Deitrick, D. Douglas, C. Gulliford, C. Mayes, J. Qiang, N. Taylor, and F. Willeke, Electron ion collider strong hadron cooling injector and ERL, in *Proceedings of the 31st International Linear Accelerator Conference, LINAC-2022, Liverpool, UK* (JACoW, Geneva, Switzerland, 2022), pp. 7–12.
- [8] H. Zhao, L. Mao, J. Yang, J. Xia, X. Yang, J. Li, M. Tang, G. Shen, X. Ma, B. Wu, G. Wang, S. Ruan, K. Wang, and Z. Dong, Electron cooling of a bunched ion beam in a storage ring, *Phys. Rev. Accel. Beams* **21**, 023501 (2018).
- [9] H. Zhao, M. Blaskiewicz, A. V. Fedotov, W. Fischer, X. Gu, D. Kayran, J. Kewisch, C. Liu, S. Seletskiy, V. Schoefer, and P. Thieberger, Cooling simulation and experimental benchmarking for an rf-based electron cooler, *Phys. Rev. Accel. Beams* **23**, 074201 (2020).
- [10] A. V. Fedotov *et al.*, Experimental demonstration of hadron beam cooling using radio-frequency accelerated electron bunches, *Phys. Rev. Lett.* **124**, 084801 (2020).
- [11] M. W. Bruker *et al.*, Demonstration of electron cooling using a pulsed beam from an electrostatic electron cooler, *Phys. Rev. Accel. Beams* **24**, 012801 (2021).
- [12] A. A. Mikhailichenko and M. S. Zolotarev, Optical stochastic cooling, *Phys. Rev. Lett.* **71**, 4146 (1993).
- [13] M. S. Zolotarev and A. A. Zholents, Transit-time method of optical stochastic cooling, *Phys. Rev. E* **50**, 3087 (1994).
- [14] J. Jarvis, V. Lebedev, A. Romanov, D. Broemmelsiek, K. Carlson, S. Chattopadhyay, A. Dick, D. Edstrom, I. Lobach, S. Nagaitsev *et al.*, Experimental demonstration of optical stochastic cooling, *Nature (London)* **608**, 287 (2022).
- [15] V. N. Litvinenko and Y. S. Derbenev, Free electron lasers and high-energy electron cooling, in *Proceedings of the 29th International FEL Conference, Novosibirsk, Russia* (BINP, Novosibirsk, 2007), p. 268.
- [16] V. N. Litvinenko and Y. S. Derbenev, FEL-based coherent electron cooling for high-energy hadron colliders, Brookhaven National Laboratory (BNL), Upton, NY, Technical Report No. BNL-81333-2008-CP, 2008.
- [17] V. N. Litvinenko, Advances in coherent electron cooling, in *Proceedings of the International Workshop on Beam Cooling and Related Topics, COOL-2013, Murren, Switzerland* (JACoW, Geneva, Switzerland, 2013), pp. 10–14.
- [18] D. Ratner, Microbunched electron cooling for high-energy hadron beams, *Phys. Rev. Lett.* **111**, 084802 (2013).
- [19] V. Litvinenko *et al.*, Coherent electron cooling experiment at RHIC: Status and plans, in *Proceedings of the 12th Workshop on Beam Cooling and Related Topics, COOL-2019, Novosibirsk, Russia* (JACoW, Geneva, Switzerland, 2019), pp. 35–40.
- [20] V. N. Litvinenko, S. Belomestnykh, I. Ben-Zvi, J. C. Brutus, A. Fedotov, Y. Hao, D. Kayran, G. Mahler,

- A. Marusic, W. Meng *et al.*, Proof-of-principle experiment for FEL-based coherent electron cooling, Brookhaven National Laboratory (BNL) Relativistic Heavy Ion Collider, Technical Report No. BNL-96405-2011-CP, 2011.
- [21] G. Wang and M. Blaskiewicz, Dynamics of ion shielding in an anisotropic electron plasma, *Phys. Rev. E* **78**, 026413 (2008).
- [22] A. Elizarov and V. Litvinenko, Dynamics of shielding of a moving charged particle in a confined electron plasma, *Phys. Rev. ST Accel. Beams* **18**, 044001 (2015).
- [23] G. I. Bell, I. Pogorelov, B. T. Schwartz, D. L. Bruhwiler, V. Litvinenko, G. Wang, and Y. Hao, Modulator simulations for coherent electron cooling using a variable density electron beam, [arXiv:1404.2320](https://arxiv.org/abs/1404.2320).
- [24] J. Ma, Numerical algorithms for Vlasov-Poisson equation and applications to coherent electron cooling, Ph.D. thesis, The Graduate School, Stony Brook University, Stony Brook, NY, 2017.
- [25] J. Ma, X. Wang, G. Wang, K. Yu, R. Samulyak, and V. Litvinenko, Simulation studies of modulator for coherent electron cooling, *Phys. Rev. Accel. Beams* **21**, 111001 (2018).
- [26] G. Wang, V. N. Litvinenko, I. Pinayev, Y. Jing, D. Kayran, J. Ma, I. Petrushina, M. Sangroula, K. Shih, and Y. H. Wu, Summary of the CeC experiment in RHIC run 21, Brookhaven National Laboratory (BNL), Upton, NY, Technical Report No. BNL-222354-2021-TECH, 2021.
- [27] D. Escande, D. Bénisti, Y. Elskens, D. Zarzoso, and F. Doveil, Basic microscopic plasma physics from N-body mechanics, *Rev. Mod. Plasma Phys.* **2**, 9 (2018).
- [28] A. Al Marzouk, H. D. Schaumburg, S. Abeyratne, and B. Erdelyi, Efficient algorithm for high fidelity collisional charged particle beam dynamics, *Phys. Rev. Accel. Beams* **24**, 074601 (2021).
- [29] A. Al Marzouk, Collisional methods with applications to charged particle beams, Ph.D. thesis, Northern Illinois University, Dekalb, IL, 2021.
- [30] A. Al Marzouk and B. Erdelyi, First benchmarked electron cooling simulations from first principles, *Nucl. Instrum. Methods Phys. Res., Sect. A* **1049**, 168092 (2023).
- [31] V. N. Litvinenko, Y. Jing, D. Kayran, P. Inacker, J. Ma, T. Miller, I. Petrushina, I. Pinayev, K. Shih, G. Wang, and Y. H. Wu, Plasma-cascade instability, *Phys. Rev. Accel. Beams* **24**, 014402 (2021).
- [32] V. Litvinenko *et al.*, Results of the coherent electron cooling experiment at RHIC, in *Proceedings of the 13th International Particle Accelerator Conference, IPAC-2022, Bangkok, Thailand* (unpublished).
- [33] A. O. Sidorin, I. N. Meshkov, I. A. Seleznev, A. V. Smirnov, E. M. Syresin, and G. V. Trubnikov, BETACOOOL program for simulation of beam dynamics in storage rings, *Nucl. Instrum. Methods Phys. Res., Sect. A* **558**, 325 (2006).
- [34] H. Zhang, J. Chen, H. Huang, R. Li, L. Luo, and Y. Zhang, Development of the electron cooling simulation program for JLEIC, in *Proceedings of the 7th International Particle Accelerator Conference, IPAC-2016, Busan, Korea* (JACoW, Geneva, Switzerland, 2016), pp. 2451–2453.
- [35] A. Latina, rf-Track Reference Manual, Zenodo 2.0.4 (2020), <https://doi.org/10.5281/zenodo.3887085>.
- [36] K. Yu and V. Samulyak, SPACE code for beam-plasma interaction, in *Proceedings of the 6th International Particle Accelerator Conference, IPAC-2015, Richmond, VA* (JACoW, Geneva, Switzerland, 2015), pp. 728–730.
- [37] VSim Tech-X Corporation (2023), <https://txcorp.com/vsim>.
- [38] A. V. Fedotov, D. L. Bruhwiler, D. T. Abell, and A. O. Sidorin, Detailed studies of electron cooling friction force, *AIP Conf. Proc.* **821**, 319 (2006).
- [39] S. Abeyratne, A. Gee, and B. Erdelyi, An adaptive fast multipole method in cartesian basis, enabled by algorithmic differentiation, *Commun. Nonlinear Sci. Numer. Simul.* **72**, 294 (2019).
- [40] A. Al Marzouk and B. Erdelyi, Collisional N-body numerical integrator with applications to charged particle dynamics, *SIAM J. Sci. Comput.* **40**, B1517 (2018).
- [41] G. Strang, On the construction and comparison of difference schemes, *SIAM J. Numer. Anal.* **5**, 506 (1968).
- [42] J. Ma, V. Litvinenko, and G. Wang, Simulations of coherent electron cooling with free electron laser amplifier and plasma-cascade micro-bunching amplifier, in *Proceedings of the 13th International Computational Accelerator Physics Conference, ICAP-2018, Key West, FL* (JACoW, Geneva, Switzerland, 2019), pp. 52–58.